Advanced Powder Technology 27 (2016) 1367–1379

Contents lists available at ScienceDirect

Advanced Powder Technology

journal homepage: www.elsevier.com/locate/apt

Original Research Paper

Comparative evaluation of normal viscoelastic contact force models in low velocity impact situations

Rimantas Kačianauskas [a,*], Harald Kruggel-Emden [b], Evaldas Zdancevičius [a], Darius Markauskas [a]

[a] Vilnius Gediminas Technical University, Lithuania
[b] Ruhr University of Bochum, Germany

ARTICLE INFO

Article history:
Received 2 October 2015
Received in revised form 16 April 2016
Accepted 27 April 2016
Available online 6 May 2016

Keywords:
Spherical particle
DEM
Viscoelastic damping
Normal contact
Coefficient of restitution

ABSTRACT

The issue of the dissipative normal nonlinear Hertz type contact, extensively explored in the discrete element simulations, is addressed. As several viscoelastic normal contact force models equally coexist, selected viscous damping models for spherical contacts (Lee and Hermann, 1999; Tsuji et al., 1992; Kuwabara and Kono, 1987; Hu et al., 2011) are investigated, and a comparative evaluation of these models in single particle and granular chain impact situations is presented. It is shown that these models can be characterised by different values of the inter-particle displacement (overlap) exponent equal to 0, 0.25, 0.5 and 1.5, respectively. A benchmarking is performed in terms of non-dimensional variables, where a variation of the damping ratio and the contact force for a wide range of coefficient of restitutions is studied. The main purpose of this study is to demonstrate the contribution of models to the propagation of force in a chain of contacting particles. Numerical results and their validation against an available experiments are given. The sensitivity of models to the impact velocity is also illustrated. Finally, based on the investigation's results, conclusions and recommendations for DEM simulations are given.

1. Introduction

The Discrete Element Method (DEM) introduced by Cundall and Strack [1] has been widely recognised as the most suitable numerical technique for simulating the behaviour of granular materials on both microscopic and macroscopic scales. As the dynamic state of a particles system on the macroscale is governed by the evolution of single contacts during (in the simplest case) binary collisions on the microscale, a simplified but still realistic description of the contact between interacting particles represents the most essential task in a DEM simulation. Generally, the contact problem of particles during binary collisions can be resolved in the framework of contact mechanics on the continuum level. The fundamentals of the contact phenomena, as well as the description of interaction laws and numerous applications may be found in Johnson [2], Wriggers [3], Matuttis and Chen [4]. Comprehensive reviews of theoretical models for various contact forces extensively used in the DEM are presented in the DEM-related works by Schäfer et al. [5], Džiugys and Peters [6], Zhang et al. [7], Lu et al. [8], and the references therein.

It is worth mentioning that, regardless of the actual particle shape, forces (torques) and displacements (rotations) in the particle contact point are usually considered by two perpendicular components normal and tangential to the contact surface. Note that our study is limited to normal contact analysis. However, it's worth to mention that there are cases when major part of energy losses could be caused by the contact force in tangential direction due to the tangential damping or friction force. This case occurs when particles velocity is relatively low and density of particles occupied volume is high.

The most important aspect attributed to DEM contact force models is the physical nature of the contact. The elastic (reversible and non-dissipative) behaviour is well understood. A collision is elastic when the contact displacement is independent of the displacement rate and any consolidation time. The elastic contact of a spherical particle in the approach and repulsion phase is described by Hertz theory [2]. A particular focus on normal contacts and extensive reviews may be found in Stevens and Hrenya [9] and Kruggel-Emden et al. [10], who studied binary collisions based on experimental data involving different material combinations and contact mechanisms.

In contrast to elastic contact behaviour, the interpretation of the dissipative behaviour in non-elastic contacts is more complicated. Usually, two dissipation mechanisms, i.e. elastic–plastic and viscoelastic, dominate in a normal contact. A plastic collision

* Corresponding author. Tel.: +370 52744854; fax: +370 52700112.
E-mail address: rimantas.kacianauskas@vgtu.lt (R. Kačianauskas).

http://dx.doi.org/10.1016/j.apt.2016.04.031
0921-8831/

leaves the involved particle permanently deformed, but the deformation of a body in this case is independent of the displacement rate (cf. [4,11]).

In the case of a viscoelastic contact, the contact deformation of particles is reversible, but the displacement itself shows a dependence on the displacement rate and possible consolidation time. In most of the earlier DEM studies, the viscoelastic contact is treated using a linear interaction model consisting of a linear spring and linear dashpot (LSD), where the dissipative behaviour is characterised by a single constant. In spite of computational simplicity, the linear model possesses physical inconsistencies such as the jump of the contact force at the beginning of the collision or the occurrence of artificial attraction and a constant impact velocity independent duration of contact (see [6,12]). To overcome some of the limitations such as the non-zero force towards the end of a contact, linear spring dashpot (LSD) models were sometime being assumed to cease when the contact force assumed a value of zero instead of the overlap being zero (cf. [13]). However, such model modifications fix only some of the problems related to LSD models [10].

Extending (LSD) models combinations of the Hertzian spring with dashpots are classified as non-linear, or Hertzian (HSD), models. Since nonlinear dashpots are constructed based on different assumptions, various viscous damping models of different complexity were elaborated theoretically and applied in DEM simulations.

It is worth noting that parameters involved into the dashpot model do not always possess clear physical meanings. The model, combining the nonlinear Hertzian spring with a linear dashpot characterised by zero exponent, which was proposed by Lee and Herrmann [14], may be also classified to the category of nonlinear models. This model [14] produces several physical inconsistencies as the linear LSD models, but offers a varying collision time [10]. A refined nonlinear damping model based on the theory of viscous-elastic continuum materials was proposed by Kuwabara and Kono [15], while an analogous formulation was later discussed by Brilliantov et al. [16]. This model is applicable to the collision of viscoelastic spheres. Tsuji et al. [17] heuristically derived a damping model, where the coefficient of restitution is independent of the initial contact velocity. It is worth noting that the HSD type Tsuji model also produces some physical inconsistencies that were observed for linear models; the collision time is however impact velocity dependent and for zero overlap the contact force is zero as expected [10]. Still, all 3 (HSD) models [14,15,17] suffer from an un-physical attractive force during the evolution of the contact. An attempt to avoid the physically incorrect attraction force has been made by Hu et al. [18], where a modification of the Tsuji model exhibiting a hysteresis without attraction was suggested. Matuttis [19] also made a suggestion to overcome the attractive force within normal force models. It was applied successfully for contacts of polygonal particles. However, the proposed model extension results in a non-continuous evolution of the contact force. The briefly discussed (HSD) models excluding the modification by Matuttis [19] are considered hereafter, and they are denoted by the abbreviations LH, KK, TS and HU, respectively.

Since direct evaluation of the physically adjustable macroscopic dissipative constants of the material is extremely difficult, the concept of the coefficient of restitution (COR) [20,21] has been extensively explored. The COR is a parameter whose value is relatively easy accessible during an impact experiment. In order to adjust the coefficients of the dissipative models, experimental data are required. Various aspects of damping in binary and to a limited extent in multiple contacts have been investigated by several authors, e.g. Luding et al. [22], Matuttis [19], Rosas et al. [23], Antypov and Elliott [24], Malone and Xu [25], Gharib and Hurmuzlu [26], Ray et al. [27]. The focus in [19,23–25] was set on evaluating the mechanisms of energy dissipation and analysing the analogies between linear and non-linear models to derive adequate parameters. It can be summarised that evaluation of damping during binary interaction is an important aspect but not the final issue as the question remains how damping affects the different coexisting force models and to answer the admittedly difficult question of which force model/models to favour from the coexisting ones in this context.

Damping plays an important role in a variety of applied problems. It should be noted that the dissipation of impact energy in a multi-particle damper [28,29] or the propagation of dynamic force waves in powder mixtures [30], soils [31,32] and silo quakes [33] can be mentioned as representative illustrations. The dissipative nature of a granular system is essentially the summed process of multiple inelastic collisions on the particle level. Therefore, a demonstration of the contribution of the damping and, more definitely of particular damping models, would be beneficial from both theoretical and practical points of view.

Note that the dissipation of energy in multi-particle systems differs, however, from what is observed in simple binary normal interactions, because in multi-particle systems energy dissipates through different mechanisms (e.g. shear, torsion, rolling). Therefore, recovery of the contribution of normal damping is not a simple task. Nonetheless, the normal contribution is usually still the strongest, especially in dynamic behaviour of particle systems [34].

Against this background, the role and essential features of viscoelastic damping during multiple normal contacts may be best illustrated by the behaviour of one-dimensional systems. Particle impact and the propagation of compression waves in granular chains of spherical particles are therefore subjects which have been studied from many points of view. Extensive work has been conducted over the past three decades to observe and analyse the wave propagation in granular media. Methodologically, most of these studies have been focused on the comparison and validation of numerical developments with the experimental results [35–38] and in enriching fundamental knowledge. Theoretical studies were aimed towards examining various aspects of the force propagation in granular media that differ considerably from the wave propagation in continuum matter. The different kinds of granular columns [22,39] and chains, such as the tapered and stepped chains [35,37,40–42] as well as disordered chains [43] are investigated apart of mono-sized chains.

The paper presents a comparative analysis of the adequacy of selected nonlinear viscous damping models. This motivates us to perform further studies on the contribution of these damping models on the particle behaviour during the single contact and extend it to a multi-particle system. The initial contribution of this research was given in conference paper [44].

Since the dynamic behaviour of contacting particles is very sensitive to many factors, the proper choice of damping models, or systematic evaluation of available model is the issue to be known before starting simulations. Here the aim, however, is to evaluate and demonstrate the contribution of different models observed in a single contact and chain impact situations. Based on these investigations, recommendations for the selection of non-linear viscoelastic models for DEM applications are given.

The paper is organised as follows. The simulation methodology and description of collision process comprising viscoelastic damping models under consideration is described in Section 2. The non-dimensional formulation with the focus on finding model specific damping ratios is presented in Section 3. Numerical results for particle impact containing comparative analysis contact force and contribution of impact velocity are demonstrated in Section 4. Simulation results for the granular chain impact are shown and discussed in Section 5.

2. Simulation methodology and description of collision process

2.1. Basics of the discrete element method

Within the DEM simulation methodology a granular medium is assumed to be a discrete set composed of a finite number N spherical visco-elastic non-cohesive particles considered as discrete elements. An arbitrary particle ($i = 1, 2, \ldots, N$) is defined by the radius R_i, the mass density ρ_i and, consequently, the mass m_i. The elastic non-dissipative properties of a particle are defined by the Young's modulus E_i and the Poisson's ratio ν_i. Viscous properties will be discussed below.

Discussion is restricted by translational motion, while an arbitrary particle i in time t is considered in the global Cartesian frame of reference. It is characterised by the position vector of the particle mass centre $\mathbf{x}_i(t)$, translational velocity $\mathbf{v}_i(t) = \dot{\mathbf{x}}_i(t) = \mathrm{d}\mathbf{x}_i(t)/\mathrm{d}t$ and acceleration $\mathbf{a}_i(t) = \ddot{\mathbf{x}}_i(t) = \mathrm{d}^2\mathbf{x}_i(t)/\mathrm{d}t^2$, where over dot stands for the time derivatives. The particle motion is described by the Newton's second law resulting in the second-order ordinary differential equation written as follows:

$$m_i\ddot{\mathbf{x}}_i(t) = \mathbf{F}_i(t), \tag{1}$$

where the vector $\mathbf{F}_i$ stands for the resultant vector of the inter-particle contact forces $\mathbf{F}_i$ and the gravity force acting on the centre of an arbitrary spherical particle i.

It is assumed that, at time $t = 0$ the particles are in positions $\boldsymbol{x}_{0,i}$ and are entering into contact with each other under the impact velocities $\boldsymbol{v}_{0,i}$. Thus, the initial conditions for Eq. (1) are as follows:

$$\boldsymbol{x}_i(0) = \boldsymbol{x}_{0,i}, \dot{\mathbf{x}}_i(0) = \mathbf{v}_{0,i}. \tag{2}$$

The inter-particle force vector $\mathbf{F}_{ij}$, at the contact point, describes the contact between the particle i and the target j. It may be expressed as a sum of the normal and tangential components, $F_{n,ij}$ and $F_{t,ij}$.

The details for explicit evaluation of the contact kinematics and forces in terms normal and tangential components of spherical particles may be found in [45–47]. The simulation was performed using the Gear predictor–corrector fifth-order integration scheme [48].

2.2. Collision setup

The collision process for the normal impact of the single particle is considered in the following manner. It is resumed that moving particle i collides the target denoted by subscript j, i.e. another sphere or plane (half-space). The target properties are defined in the same manner as impacting particle by material parameters ρ_j, E_j, ν_j and radius R_j, respectively. For the case of a plane $R_j = \infty$. The particle-target system is characterised by the effective mass $(m_{eff})^{-1} = (m_i)^{-1} + (m_j)^{-1}$, the effective radius $(R_{eff})^{-1} = (R_i)^{-1} + (R_j)^{-1}$ and the effective elasticity modulus $(E_{eff})^{-1} = (E_i/(1-\nu_i^2))^{-1} + (E_j/(1-\nu_j^2))^{-1}$ of the contacting partners.

The collision process is illustrated in Fig. 1a, where three characteristic positions, i.e. the initiation of the contact, transition from compression to restitution and rebound, are shown. The deformation behaviour of particle in time during contact is characterised by the inter-particle displacement $h(t)$ meaning overlap of the collision partners. Collision starts at time instant t_0. The reference time $t_0 = 0$ is assumed for the sake of convenience. The compression phase is characterised by the increase of the displacement from zero until maximal value $h_{\max}$ and lasts in time interval between t_0 and t_{comp}. The restitution phase is characterised by the decrease of the displacement until full rebound and lasts in time interval from t_{comp} until t_r. Thus, the contact period during collision T_c, lasting between t_0 and the time instant of rebound t_r, is defined as $T_c = t_r - t_0$.

2.3. Evaluation of normal contact

The contact force acting on the colliding particles in the normal direction may be defined by scalar quantities. The normal component presents the repulsion force:

$$F_{n,ij}(t) = F_{el}(t) + F_{diss}(t), \tag{3}$$

where F_{el} and F_{diss} are elastic and dissipative force components, respectively.

In fact, the normal contact between two particles is modelled by a combined nonlinear spring and dashpot model (Fig. 1b).

The elastic behaviour of the normal contact is modelled by a one-dimensional axial spring. The constitutive model expresses the relationship between the conservative repulsion force F_{el} and contact displacement, i.e. particle's overlap $h(t)$. In the case of the Hertz contact law, $F_{el} = F_{Hertz}$, this relationship is nonlinear:

$$F_{Hertz}(t) = K_{eff} \cdot (h(t))^{3/2}, \tag{4}$$

Contact properties are characterised by the effective axial spring stiffness constant:

$$K_{eff} = \frac{4}{3} E_{eff} \cdot (R_{eff})^{1/2}, \tag{5}$$

which is predefined by the effective Young's modulus and the effective particle radius.

The dissipative behaviour of the dashpot is characterised by the dissipative force F_{diss}. The relationship between the force F_{diss} and overlap rate (velocity) $\dot{h} = dh/dt$ at the contact point of the colliding partners is defined as follows:

$$F_{diss}(t) = C(h(t))\dot{h}(t). \tag{6}$$

This relationship is characterised by the resultant damping parameter C, which reflects dissipative properties of both colliding partners related to internal friction, or viscosity. It depends also on their elasticity properties, masses as well as geometries and even on factors of heuristic origin yielding final expressions for the resultant damping parameter $C = C(m_{eff}, K_{eff}, h(t), \ldots)$.

2.4. Viscoelastic damping models

To generalise our approach, selected viscoelastic damping models will be considered describing them separately. The selected are denoted hereafter by subscript k (k = LH, TS, KK, HU). Focussing on the contribution of the elastic deformation, an explicitly defined generalised power-law dependency $C_k(h(t)) = C_k(h(t)^{\beta_k})$ of the damping parameter against the displacement h is manifested as:

$$C_k(h(t)) = C_{\mathrm{mod},k} \cdot \left(h(t)^{\beta_k}\right). \tag{7}$$

Here subscript k denotes the particular model, while power factor β_k presents a displacement exponent, which correlates the contribution of the elastic properties to the overall dissipative behaviour. Hence, this expression serves the formal unified template for investigation of separate damping models. This approach conceptually assumes viscous dissipation term depending on elastic deformation, see Hunt and Crossley [20].

Facing the difficulties to distinguish physically adjustable damping constants C in Eqs. (6) and (7), we can follow the traditional path expressing them via another non-dimensional parameter, the coefficient of restitution (COR). The normal COR denoted by e is defined as a scalar quantity ($0 < e < 1$), which relates the normal

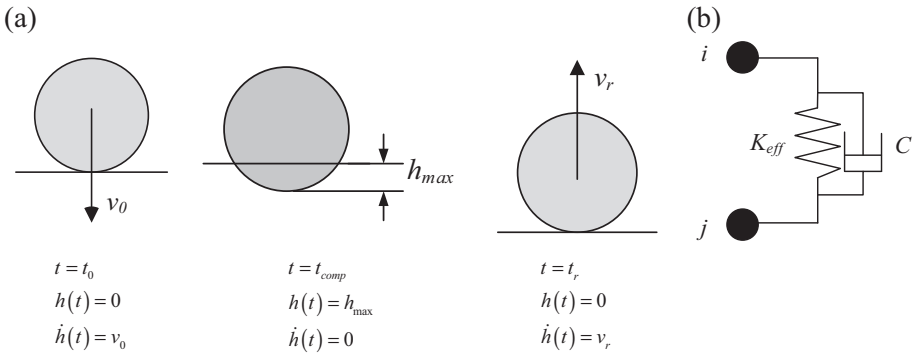

Fig. 1. Setup of normal viscoelastic collision: (a) characteristic positions of colliding particle in time and (b) constitutive interaction models.

component of the impact velocity $v_0 = \dot{h}(t_0)$ and the rebound velocity $v_r = \dot{h}(t_r)$ after the collision defined at time instant t_r, as:

$$e = \dot{h}(t_r)/v_0. \tag{8}$$

The evaluation of the relationship between the damping constants C_k for each model k and the COR e will be discussed below.

The simplest and also most popular dissipative model is the linear dashpot model based on the linear dependency between of the force and the displacement rate. The contact model combining linear dashpot model with the non-linear Hertz spring was proposed by Lee and Hermann [14]. Originally in [14], the damping model was defined by a simple expression:

$$C_{LH} = \gamma_{LH} \cdot m_{eff}. \tag{9}$$

It is easy to find, that the resultant damping parameter of the LH model $C_{LH}(h) = C_{LH}(h^0)$ may be considered as particular case of general model (7) containing zero contribution of elastic deformation, i.e., $\beta_{LH} = 0$. Here, γ_{LH} is the characteristic model relevant constant controlling dissipation, which is originally treated as an adjustable parameter. A compact expression of the COR in terms of semi-analytical approximations is recently provided by Ray et al. [27].

Another non-linear model was proposed by Tsuji et al. [17]. The TS model is characterised by the displacement exponent $\beta_{TS} = 1/4$, where the load varying resultant viscous damping constant is defined heuristically by the expression:

$$C_{TS}(t) = \gamma_{TS} \cdot m_{eff}^{1/2} \cdot (K_{eff})^{1/2} \cdot (h(t))^{1/4}. \tag{10}$$

Here, the effective stiffness K_{eff} stands for the Hertz stiffness defined according to Eq. (5), while the viscous damping constant γ_{TS} has to be known in advance. Tsuji [17], demonstrated that γ_{TS} is non-dimensional empirical constant independent on the combination of mass m_{eff} and stiffness K_{eff}, and it is uniquely related to the coefficient of restitution e. The latest relationship $\gamma_{TS}(e)$ is demonstrated originally by graphical plot. An analytical expression of them analogously to the linear model is given by several authors, e.g. [18,24], as follows:

$$c_{TS}(e) = -\frac{\sqrt{5}\ln e}{\sqrt{\ln^2 e + \pi^2}}. \tag{11}$$

The nonlinear damping model proposed by Kuwabara and Kono [15] is characterised by the exponent½. The original expression of the resultant damping parameter $C_{KK}(t)$ for this model is defined as follows:

$$C_{KK}(t) = \gamma_{KK} \cdot K_{eff} \cdot (h(t))^{1/2}. \tag{12}$$

It involves stiffness K_{eff}, displacement $h(t)$ and viscous damping constant γ_{KK}, which is originally thought to be a function of the Young's modulus, Poisson's ratio and two analogously defined viscous constants of material associated with volume and shear deformation. The theoretical continuum-based explanation of the dissipative term by exploring dissipative part of the stress tensor is given by Brilliantov et al. [16], where the relationship between γ_{KK} and the above mentioned material constants is derived analytically. Due to difficulties in obtaining of their values, dissipation parameter is fitted as a function of COR, while a tabular form of it is given originally by Kuwabara and Kono [15].

The damping model proposed and analysed by Hu et al. [18] is characterised by:

$$C_{HU}(t) = \gamma_{HU} \cdot K_{eff} \cdot (h(t))^{3/2} \cdot v_0^{-1}. \tag{13}$$

Eq. (13) was derived as an attempt to avoid non-physical attraction. Here, γ_{HU} is non-dimensional damping constant. In addition, the analytical approximate expression is given for damping ratio as follows:

$$c_{HU}(e) = -\frac{6.66264 \ln e}{3.85238 + \ln e}. \tag{14}$$

Here, the domain of the COR is defined between 0.05 and 1.0.

The underlying Eqs. (9), (10), (12) and (13) are presented in unified format where contribution of overlap is clearly distinguished. However, deeper physical explanation and the role of other factors remains beyond the scope of this investigation.

2.5. Equation of collision motion

To compare various damping models, a single particle impacting a target is considered as the first setup. The equation of motion (1) is simplified and transformed into the one-dimensional case. Regarding the previous notation for the dissipative force, the motion of particle during impact is expressed in terms of the overlap $h(t)$ and is rewritten as:

$$\ddot{h}(t) + \frac{K_{eff}}{m_{eff}}(h(t))^{3/2} + \frac{C_k(h(t))}{m_{eff}}\dot{h}(t) = 0, \tag{15}$$

while the initial conditions in Eq. (2) are transformed into the following form:

$$h(0) = 0, \quad \dot{h}(0) = v_0. \tag{16}$$

This model forms the basis for the impact analysis.

3. Non-dimensional analysis for particle impact

3.1. Modelling approach

To generalise our approach, particle collision described by Eq. (15) will be considered in a non-dimensional form. To proceed non-dimensional analysis, the non-dimensional variables such as

the relative time $\bar{t}$, the time dependent inter-particle contact displacement $\bar{h}(\bar{t})$, displacement rate $\dot{\bar{h}}(\bar{t})$ and acceleration $\ddot{\bar{h}}(\bar{t})$ are introduced in conventional form, [17,21,49]. Two independent dimensional parameters, the length parameter L and the velocity parameter v_0, form the basis of the dimensional analysis.

The characteristic length L is the maximal compression overlap for the equivalent undamped (elastic) Hertz contact problem. In our case, the scaling parameter L is defined explicitly in terms of three dimensional constants such as effective stiffness K_{eff}, mass m_{eff} and impact velocity v_0 by the expression:

$$L = a^{2/5} \cdot (K_{eff})^{-2/5} \cdot (m_{eff})^{2/5} \cdot (v_0)^{4/5}, \tag{17}$$

where the coefficient $a = (5/4)$ is related to the elastic Hertz contact.

The non-dimensional time $\bar{t} = t/T$ is scaled by time parameter T, which is related to length L by the impact velocity v_0:

$$T = L/v_0. \tag{18}$$

Eq. (18) means the time during which the particle approaches the target by distance of characteristic length. More definitely the time parameter is related to duration of Hertz contact $T = T_{Hertz}/2.94$.

On the basis of Eqs. (17) and (18), the non-dimensional motion variables are defined as:

$$\bar{h}(\bar{t}) = \frac{h(\bar{t})}{L}, \tag{19}$$

$$\dot{\bar{h}}(\bar{t}) = \frac{\dot{h}(\bar{t})}{v_0}, \tag{20}$$

$$\ddot{\bar{h}}(\bar{t}) = \frac{\ddot{h}(\bar{t}) \cdot L}{v_0^2}. \tag{21}$$

Substituting the new notation into the dimensional equation of motion (15), the desired non-dimensional form of this equation is obtained:

$$\ddot{\bar{h}}(\bar{t}) + a \cdot (\bar{h}(\bar{t}))^{3/2} + a_1 \cdot c_k(e) \cdot (\bar{h}(\bar{t}))^{\beta_k} \cdot \dot{\bar{h}}(\bar{t}) = 0. \tag{22}$$

Here the non-dimensional factor $a_1 = a^{(2(1+\beta_k)/5)}$ is defined as a model dependent quantity.

The non-dimensional Eq. (21) demonstrates that the damping properties of the above phenomenological models are expressed by the non-dimensional model-specific parameter, damping ratio c_k which is uniquely defined by the value of COR.

Analogously, initial conditions in Eq. (16) are also transformed into non-dimensional form as follows:

$$\bar{h}(0) = 0; \quad \dot{\bar{h}}(0) = 1. \tag{23}$$

3.2. Specification of damping parameters

It is obvious that for the comparison of the damping effect produced by different damping models, a unified treatment is required. From the above considerations follows that each of the damping models are characterised, as defined in Eqs. (9)–(13), by the original model-specific resultant damping parameters $C_k = C_k(\gamma_k)$ denoted by capital C being related material specific damping ratios constants γ_k. On the other hand, the non-dimensional Eq. (21) implies the occurrence of the non-dimensional damping ratios denoted with $c_k(e)$ being uniquely predefined by specified values of COR.

Two issues have to be resolved to complete specification. The first issue concerns an evaluation of the relationship $c_k(e)$. In most of the practical cases, the fitted, but not the exact analytical expressions, see Ray et al. [27], for this relationship exists. In numerical modelling, the opposite situation occurs, and an inverse relationship $c_k(e)$ is calculated. Thereby, the rebound velocity $\dot{h}(T_c)$ is obtained by solving Eq. (8) for the known values of the damping ratio c_k and the specified impact velocity v_0. As a result of a series of numerical single particle numerical impact experiments is required for calculating of the relationship $c_k(e)$ according to the definition of the COR in Eq. (8).

The second issue is how to employ the non-dimensional solution of Eq. (21) for DEM simulations. To resolve this issue, the alternative expressions of model specific expression of the global dimensional damping parameter $C_{\mathrm{mod},k} = C_{\mathrm{mod},k}(e)$ could be obtained by a backward substitution procedure. The modified expression now reads:

$$C_{\mathrm{mod},k}(e) = c_k(e) \cdot m_{eff}^{\beta_{m,k}} \cdot K_{eff}^{\beta_{K,k}} \cdot v_0^{\beta_{v,k}}. \tag{24}$$

Here, $\beta_{m,k}$, $\beta_{K,k}$, and $\beta_{v,k}$, are power factors of mass, stiffness and impact velocity which values can be extracted from the expressions given in Table 1.

The original Eqs. (9)–(13) and modified Eqs. (25)–(28) of the resultant damping parameters for all models are given in Table 1 for convenience. The treatment of damping parameters is performed by applying the following algorithm:

- Selection of expressions for the damping parameter according to Eqs. (9)–(13), column 3 in Table 1.
- Definition of non-dimensional variables by scaling the length with the length parameter L and the velocity with the parameter v_0.
- Transformation of the dimensional Eq. (15) into a non-dimensional form: Eq. (21), with non-dimensional damping ratios $c_k(e)$.
- Evaluation of damping ratios by solving the inverse problem numerically using the non-dimensional equation of motion (22) with initial conditions in Eq. (23).
- Evaluation of the resultant modified damping parameters $C_{\mathrm{mod},k}$ for the specified value of e according to the modified Eqs. (25)–(28) given in column 5 of Table 1.

3.3. Numerical calculation of the damping ratios

The aforementioned approach was explored for the illustration of damping models, where the relationship between 2 decisive characteristics, the non-dimensional damping ratio c_k and the coefficient of restitution e is obtained. Each of the 4 models characterised by different values of the displacement exponent β_k was considered in this study. As a final result, 4 relationships were calculated numerically. In order to obtain the specified point on the curve $c_k(e)$, numerical experiments comprising the calculation of the entire compression-restitution cycle until full rebound are necessary. Simulation results are given in Fig. 2.

It is worth noting that the above non-dimensional relationships are universal and uniquely defined. They have been separately considered by different authors. It could be stated, however, that a simple analytical solution for the nonlinear HSD model is still not found. Consequently, only comparison with fitted, asymptotic or numerical solutions is available. Examination of the numerically obtained results plotted in Fig. 3 shows that the damping ratio $c_{TS}(e)$ obtained for the Tsuji model perfectly matches analytical expression. Eq. (11), where $c_{HU}(e)$ is obtained for the Hu model, matches the fitted Eq. (14) as it was originally presented in [18]. The damping ratio $c_{LH}(e)$ obtained for the Lee and Hermann model matches expression obtained for the case of the linear solution, [6,18]. The $c_{KK}(e)$ obtained numerically gives satisfactory coincidence with the results originally presented by Kuwabara and Kono [15] in tabular form.

Table 1
Summary of the analytical expressions of damping parameters for various models.

k	β_k	Original expression of resultant damping parameter C_k	Eq. no.	Modified expression of resultant damping parameter $C_{\mathrm{mod},k}$	Eq. no.
LH	0	$C_{LH} = \gamma_{LH} \cdot m_{eff}$	(9)	$C_{\mathrm{mod},LH} = c_{LH}(e) \cdot m_{eff}^{3/5} \cdot K_{eff}^{2/5} \cdot v_0^{1/5}$	(25)
TS	1/4	$C_{TS}(t) = \gamma_{TS} \cdot m_{eff}^{1/2} \cdot K_{eff}^{1/2} \cdot (h(t))^{1/4}$	(10)	$C_{\mathrm{mod},TS} = c_{TS}(e) \cdot m_{eff}^{1/2} \cdot K_{eff}^{1/2}$	(26)
KK	1/2	$C_{KK}(t) = \gamma_{KK} \cdot K_{eff} \cdot (h(t))^{1/2}$	(12)	$C_{\mathrm{mod},KK} = c_{KK}(e) \cdot m_{eff}^{2/5} \cdot K_{eff}^{3/5} \cdot v_0^{-1/5}$	(27)
HU	3/2	$C_{HU}(t) = \gamma_{HU} \cdot K_{eff} \cdot (h(t))^{3/2} \cdot v_0^{-1}$	(13)	$C_{\mathrm{mod},HU} = c_{HU}(e) \cdot K_{eff} \cdot v_0^{-1}$	(28)

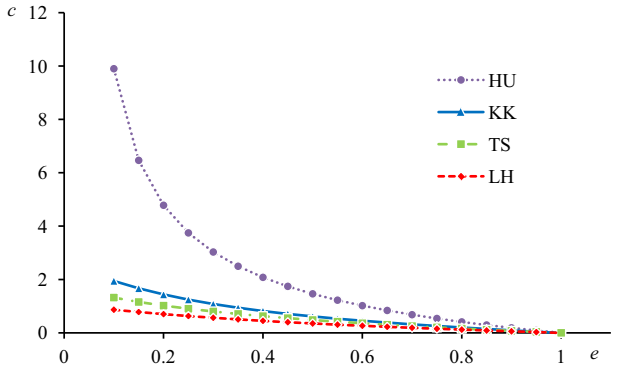

Fig. 2. Numerically obtained relationship between the damping ratios $c_k(e)$ and the COR values for various damping models.

4. Numerical analysis for particle impact

4.1. Evaluation of contact force

The contribution of damping until now was basically limited by discussion about damping constants. The role and consequences of using an appropriate damping model to the values of inter-particle forces will be considered in this subsection. The maximum value of the contact force occurring during the entire compression-restitution cycle of the single particle colliding the target will be discussed in detail. Here, another component of the full solution namely time history of acceleration will be explored.

Actually, the equilibrium of forces during motion allows one to interpret the inertia force as the resultant of the elastic and damping forces. Consequently, the total normal non-dimensional contact force may be considered in terms of the non-dimensional accelerations extracted from the simulation of the single particle impact experiment:

$$\bar{F}_n(\bar{t}) = \ddot{\bar{h}}(\bar{t}), \tag{29}$$

where the effective mass is assumed to be equal to unity.

Regarding definition of acceleration in Eq. (21), the dimensional inter-particle force is:

$$F_n(\bar{t}) = m_{eff}(v_0^2/L)\ddot{\bar{h}}(\bar{t}). \tag{30}$$

Regarding these notations, numerical force analysis is focussed on the analysis of acceleration $\bar{a}(\bar{t}) \equiv \ddot{\bar{h}}(\bar{t})$. Time histories of acceleration $\bar{a}(\bar{t})$ for all four damping models are shown by graph in Fig. 3, where two families of curves illustrate forces obtained for two values of COR $e = 0.8$ (Fig. 3a) and $e = 0.4$ (Fig. 3b), respectively. Purely elastic behaviour obtained by the Hertz model is also given for the sake of comparison. Physical interpretation of the obtained forces in terms of acceleration–displacement relationship $\bar{a}(\bar{t}) - \bar{h}(\bar{t})$ is given in Fig. 4. Here, a positive displacement and force indicates compression.

The graphs show that an increase of the exponent β for displacement h, i.e., h^β systematically yields increase of the values of the maximal normal interaction force occurring at the end of compressive loading stage. In the case of the relatively high restitution when $e \geqslant 0.8$, this contribution remains, however, relatively small (Figs. 3a and 4a). The presence of damping reduces the non-dimensional value of elastic acceleration (force) equal to $\bar{a}_{Hertz} = 1.25$ up to $\bar{a}_{HU} = 1.14$ for HU model and up to $\bar{a}_{LH} = 0.98$ for LH model. Contribution of damping with decreased restitution e = 0.4 (see Figs. 3b and 4b) yields a reduction of the force up to $\bar{a}_{HU} = 1.22$ for HU, $\bar{a}_{KK} = 0.97$ for KK, $\bar{a}_{TS} = 0.91$ for TS, $\bar{a}_{LH} = 0.87$ for LH and differences between different model behaviours.

We are interested generally in effects yielded by different damping models for broader range of parameters. Variations of maximal forces against the COR are additionally illustrated in Fig. 5. The graphs confirm drop of these values and the increasing differences between forces in systematic fashion when COR values drop below 0.8. Only the exceptional result obtained by the HU model could be remarked upon.

Generally, an increase of the displacement exponent in the damping models changes the proportion between the compression and restitution periods and leads to an increase in the total contact duration. Due to different deformation rates after impact, the

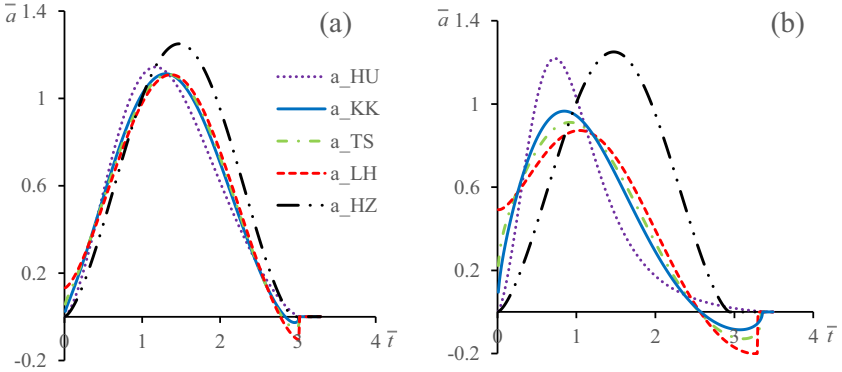

Fig. 3. Time histories of the non-dimensional acceleration $\bar{a}(\bar{t})$ during single particle impact for various viscoelastic models obtained at different values of the coefficient of restitution: (a) $e = 0.8$; (b) $e = 0.4$.

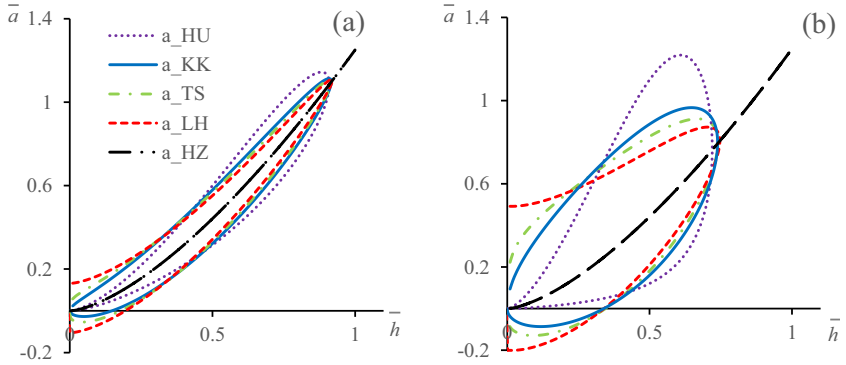

Fig. 4. Non-dimensional acceleration–displacement relationship $\bar{a}(\bar{t}) - \bar{h}(\bar{t})$ during single particle impact for various viscoelastic damping models obtained at different values of the coefficient of restitution: (a) $e = 0.8$; (b) $e = 0.4$.

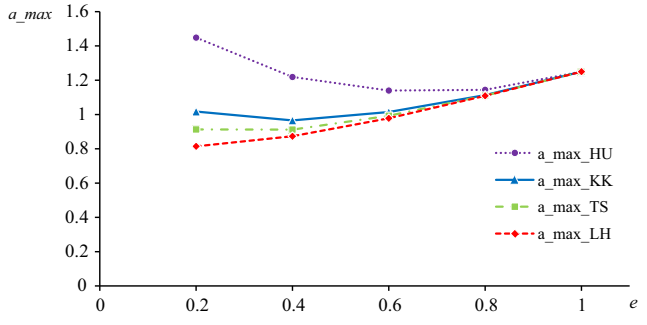

Fig. 5. Numerically obtained relationship between the maximum acceleration and the COR e for various damping models.

increase of overlap not only during loading but also continues at the initial stage of unloading, while maximum overlap. This lack of proportion increases with the drop of the COR value. It could be stated that the force values obtained by TS and KK models are enveloped by values of LH and HU models.

The highest dissipative contribution is exhibited by the LH model when the role of the contact displacement is neglected. The results give a clear indication about the role of particular damping model to the values of the inter-particle force. The importance of these results may be even higher if force values approached physical limits causing contact plasticity or damage, consequently, the selection of damping model may contribute physical results.

4.2. Comparison of models against experimental results

Classification of damping models addressed in Section 3 according to displacement exponent reflects rather relative interrelationship among different damping models. Their correspondence to reality remains, however, unclear. Consequently, an appropriate reference label is required to tie this relative scaling, therefore, comparison of models against experimental results would indicate their adequacy to reality.

Result of a collision experiment using a pendulum device reported by Van Zeebroeck et al. [50] will be explored for these purposes. It could be noticed that such a detailed presentation of experiment data accessible on this level is very limited.

The experimental setup is based on a pendulum device consisting of a long arm with an aluminium impactor, where an aluminium half sphere of radius $R_{im} = 25$ mm is an impacting collider striking the rubber half sphere of radius $R_j = 41.5$ mm fixed on the anvil. In this impact experiment, the starting time t_0 is equal to zero, and recording of results has been interrupted close to the end of the collision.

A comparison of simulation results against the experiment in terms of time histories is presented in Fig. 6, where variations of normal force, displacement rate and displacement versus time are shown in Fig. 6a–c, respectively. Experimental curves are reproduced directly from images given in figures presented by Van Zeebroeck [50].

It is worth noting in advance that the presentation of simulation results is much more complicated in reality, because some data could not be found directly. The experimental velocity curve directly yields the values of the impact, $v_0 = 0.2$ m/s, and rebound, $v_r = 0.135$ m/s, velocities, respectively. As a consequence, the value of the coefficient of restitution $e = 0.674$ is calculated directly by Eq. (8). The value of contact stiffness $K = 3.950 \cdot 10^5$ N m$^{-3/2}$ and the modified damping constant $C_{\mathrm{mod},KK} = 6.88 \cdot 10^2$ kg m$^{-1/2}$ s^{-1} are extracted from [50]. This value of $C_{\mathrm{mod},KK}$ was also proved by applying the modified Eq. (27), where with $c_{KK}(0.674) = 0.351$ obtained from the graph on Fig. 2 is substituted. These values were used to calculate the graphs on Fig. 6 reflecting theoretical KK model. The value of mass is obtained explicitly from the modified damping constant Eq. (27) $m_{eff} = 0.306$ kg.

Force and displacement show a sinusoidal shape. The displacement rate shows a change of sign, whereas the initial displacement rate is larger than the terminal velocity due to dissipation. It became obvious that the graphs in Fig. 6 lead to important statement showing the force obtained by KK model data being below experimental results.

Consequently, the HU models were examined in the same manner. The value of damping ratio $c_{HU}(0.674) = 0.760$ is deduced from the graph in Fig. 2. The resultant damping constant is evaluated according to the modified Eq. (28), which yields the value $C_{\mathrm{mod},HU} = 1.50 \cdot 10^6$ kg m$^{-3/2}$ s^{-1}.

From these results, it follows that the maximal value of the interaction force observed experimentally $F_{\mathrm{max,exp}} = 12.1$ N is enveloped by the values $F_{\mathrm{max},KK} = 11.8$ N and $F_{\mathrm{max},HU} = 12.7$ N obtained according to the KK and HU models, thus $F_{\mathrm{max},KK} \leqslant F_{\mathrm{max,exp}} \leqslant F_{\mathrm{max},HU}$.

4.3. Contribution of the impact velocity

It is already known that damping is complicated phenomenon depending on several factors. In contrast, the DEM presents a simulation tool developed on the basis of simplified assumptions, where the normal component is characterised by the single non-measurable dashpot parameter, in our case, the global damping model k depending constants C_k. In the most of the DEM applications it is uniquely defined by the fixed values of the coefficient of restitution $C_k(e)$.

Investigations relating DEM simulations and experimental observations in terms of the variable COR and/or non-uniquely

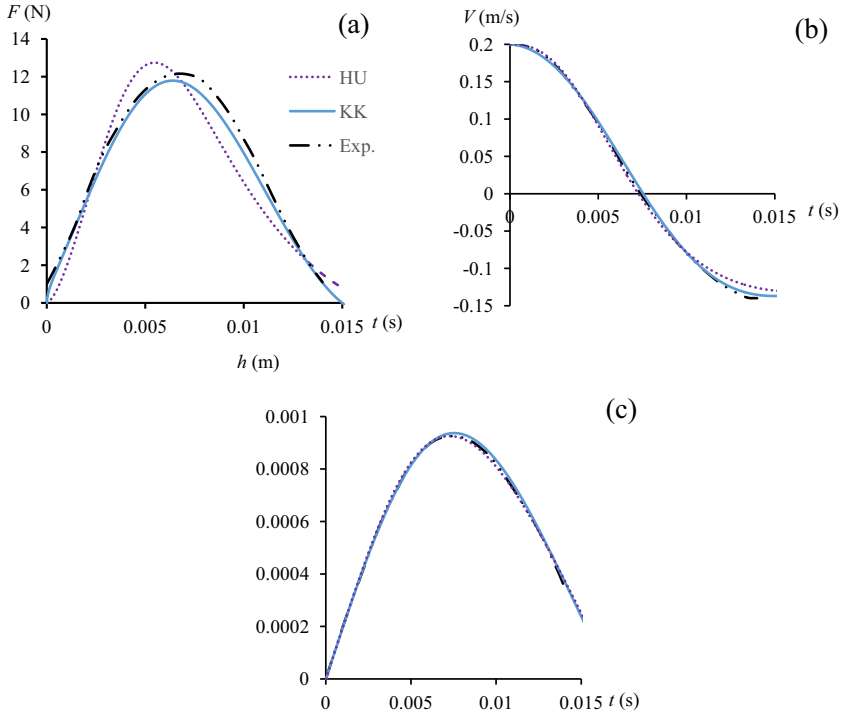

Fig. 6. Comparison of selected viscoelastic models defined by coefficient of restitution $e = 0.674$ with experimental results obtained by Van Zeebroeck et al. [2] during contact of an aluminium half sphere impacting a rubber half sphere: (a) force versus time; (b) velocity versus time; (c) displacement versus time.

defined damping constant are rather limited. Experiments, [9,10], as well as theoretical investigations [21,51] provide the evidence that the COR is an impact velocity-dependent quantity, therefore not only COR contributes damping properties. In particular, the new approach adjusted for different materials and comprises an extension of the non-linear normal damping force models by fitting the contact stiffness, the dashpot damping coefficient and, additionally, the exponent of the displacement rate was suggested in [10]. The new developed models were expected directly be used in DEM simulations. The issue of impact velocity in DEM simulations of multi particle vibrated systems is discussed and illustrated by McNamara and Falcon [51].

One of the purposes of this study to illustrate how the contribution of the impact velocity could or should be treated in DEM simulations in the context of different damping models. Equations of the modified damping constants (25)–(28) obtained by applying dimensional analysis give evidence of how the value of impact velocity contributes the damping parameters. As it follows from Eqs. (25)–(28), the values of the modified damping constant $C_{\mathrm{mod},k}(e, v_0)$ may be expressed in terms of the pair of coupled parameters, the COR and the impact velocity, where coefficient of restitution e is attributed to the specified value of the impact velocity termed hereafter as reference velocity $v_{0,ref}$. The reference velocity is computational parameter which value is measured by evaluation of COR in experiment. Concerning the role of impact velocity, it could be observed that each of the damping models shows different sensitivity to the variation of impact velocity which may be characterised by another parameter. The power factor (exponent) of impact velocity has the values of $\beta_{v,LH} = 1/5$, $\beta_{v,TS} = 0$, $\beta_{v,KK} = -1/5$ and $\beta_{v,HU} = -1$ for each of the models.

It could be stated, however, that in multi-particle systems actual value of the impact velocity v_0 between particles is not known a priori. This velocity varies in time, The value of impact velocity applied during simulations is termed hereafter as the simulation velocity $v_{0,sim}$. It is assumed that the unknown value of this velocity could be hypothetically specified in advance basing on heuristic arguments, and it is different than $v_{0,ref}$.

The relative variation of the actual velocity could be evaluated by introducing a dimensionless variable λ:

$$\lambda = v_{0,ref}/v_0. \tag{31}$$

Using the above Eq. (31), a general expression of the modified damping constant $C_{\mathrm{mod},k}(e, v_0)$, i.e. Eq. (24), could be corrected with respect to simulation velocity as $C_{\mathrm{mod},k}(e, v_{0,sim})$ and expressed in terms of parameter $\lambda_{sim} = v_{0,ref}/v_{0,sim}$ as follows:

$$C_{\mathrm{mod},k}(e,\lambda) = c_k(e)\cdot\lambda_{sim}^{\beta_{v,k}}\cdot m_{eff}^{\beta_{m,k}}\cdot K_{eff}^{\beta_{K,k}}\cdot v_{0,ref}^{\beta_{v,k}}. \tag{32}$$

Here, $\lambda^{\beta_{v,k}}$ may be treated as damping ratio correction factor, while

$$c_{\mathrm{corr},k}(e,\lambda) = c_k(e)\lambda^{\beta_{v,k}}, \tag{33}$$

is the impact velocity corrected damping ratio. Using Eqs. (31)–(33), Eqs. (25)–(28) could be corrected in the same manner.

In the particular case, $v_{0,ref} \approx 1$ m/s and $\lambda_{sim} = 1$, which is characteristic for many impact experiments, the absolute values of simulation and reference impact velocities are insignificant. Eq. (32) could by applied for evaluation of the role of impact velocity in damping models, consequently, the above particular case serves for velocity independent damping constant.

The contribution of impact velocity is illustrated in Fig. 7. Variations of correction factors $\lambda^{\beta_{v,k}}$ for various damping models against the relative impact velocity λ are shown in Fig. 7a.

A practical illustration of the impact velocity is given by considering the damping properties of the stainless steel (grade 316) reported by Stevens and Hrenya [9]. The dissipative properties of the contacting spherical particles are defined by experimentally obtained curve shown in Fig. 7d, where the specified values of the coefficient of restitution e are presented as the impact velocity v_0 dependent quantities. Assuming the reference impact velocity $v_{0,ref} = 1.0$ m/s and $\lambda_{sim} = 1$, the corresponding value of the

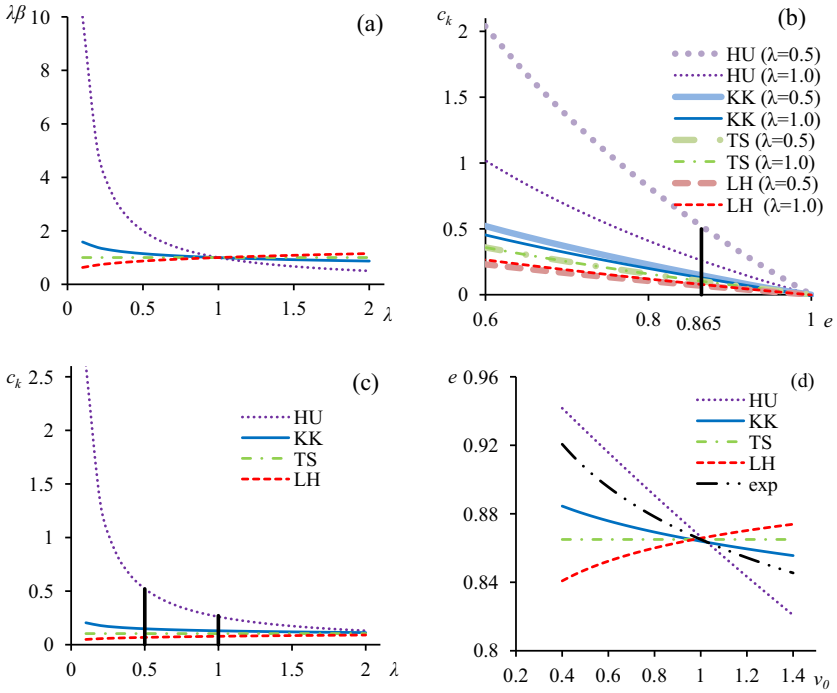

Fig. 7. Contribution of the impact velocity: (a) variations of the correction factors $\lambda^{\beta_{v,k}}$ against impact factor λ, (b) variations of damping ratios against COR at fixed values of the relative velocity $\lambda_{sim} = 0.5$ and $\lambda = 1$, (c) variations of damping ratios against relative impact velocity at fixed value of COR $e = 0.865$, and (d) variation of the COR against impact velocity.

coefficient of restitution $e = 0.865$ was found. The damping ratios $c_k(0.865)$ corresponding to this value are extracted from the graphs on Fig. 2, and the following values, $c_{LH}(0.865) = 0.078$, $c_{TS}(0.865) = 0.103$, $c_{KK}(0.865) = 0.129$ and $c_{HU}(0.865) = 0.261$, are obtained for various damping models.

Furthermore, Eq. (33) was applied to evaluate sensitivity of damping parameters in the vicinity of this reference point. Contribution of the impact velocity to damping ratios is illustrated in Fig. 7b and c. Variations of damping ratios $c_k(e, \lambda_{sim})$ against COR at fixed value $\lambda_{sim} = 0.5$ are given in Fig. 7b, where they are denoted by dashed lines. Initial variations of $c_k(e, \lambda)$ obtained at $\lambda_{sim} = 1$ already given in Fig. 2 are also shown by solid lines for the sake of comparison. Deviations of damping ratios against relative impact velocity at fixed value of COR $c_k(e, \lambda)|e = 0.865$ are given in Fig. 7c. It is obvious that these graphs mimic Fig. 7a, while new values of damping exhibiting, however, reduced deviations. In particular, reduction of the impact velocity from 1.0 up to 0.5 m/s increases damping ratios $c_{KK}(0.865) = 0.129$ of KK model up to 0.148 and $c_{HU}(0.865) = 0.261$ of HU model up to 0.522. In contrast, for the LH model, damping ratio $c_{LH}(0.865) = 0.078$ is reduced up to 0.068.

The values of COR obtained by applying Eq. (32) are shown in Fig. 7d, where the experimentally obtained curve [9] of COR is given for the sake of comparison. In Fig. 7d it is clearly seen that none of the models can match the experiment curve. The graph illustrates that the experimentally obtained value of the COR is enveloped by KK and HU models. This tendency for some of models was already indicated in [9].

On the basis of the above results, it is obvious that the Tsuji model characterised by $\beta_{v,TS} = 0$ is insensitive to variation of impact velocity. The mostly used Kuwabara and Kono model with $\beta_{v,KK} = -1/5$ as well as Lee and Herrmann model with $\beta_{v,LH} = 1/5$ yields a reasonable contribution of impact velocity and deviation from the Tsuji model. The Hu model with $\beta_{v,HU} = -1$ examined originally [18] at impact velocity $v_0 = 6.3$ m/s exhibits, however, enormous deviations of kinetic energy dissipation at velocities below 1 m/s.

5. Impact of granular chain

5.1. Impact setup

The interaction behaviour between 2 grains during impact plays a fundamental role in transferring forces from particle to particle and propagation of dynamic waves in granular systems. The treatment of granular materials differs, however, from the two-particle interaction because the process of multiple collisions dominates in the system's dynamic behaviour. Although the dynamic evolution of the external excitations depends on the nature of the granules, the character of initial disturbance and a number of other factors, its essential features may be illustrated by the behaviour of one-dimensional chain of spherical particles. Propagation of the wave in the granular chain particles in impact situations is investigated to demonstrate available differences caused by different damping models in the case of multiple contacts.

Two types, the mono-sized and the stepped chains of spherical particles (Fig. 8) will be considered here. At the very beginning, the chain particles are located touching each other with the zero initial gap without the precompression and with zero initial velocities. The chain is impacted by a striker having the impact velocity v_0.

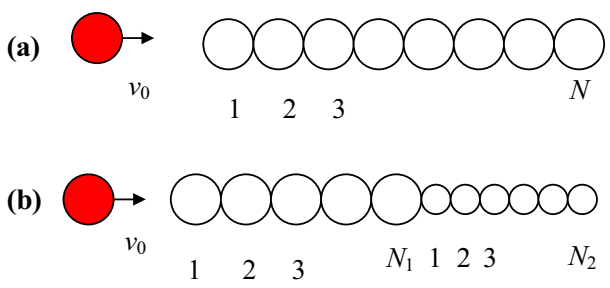

Fig. 8. Setup of granular chain impact: (a) mono-sized chain; (b) stepped chain.

The striker, which is shaded in Fig. 8, presents spherical particle having radius R_{str}.

The stepped chain (Fig. 8b) consists of parts. Thus, the first part of the chain contains N_1 number of larger particles having radius R_1, while the second part consists of N_2 the smaller particles with the radius R_2, where $R_2 < R_1$. The chain of mono-sized particles (Fig. 8a) presents the particular case of the stepped chain, where the second part is simply ignored.

The chain is treated as granular system, and the standard DEM approach was explored for simulation purposes. By neglecting gravity and inter-particle friction, only one-dimensional translational motion occurs by solving Eq. (1). Interaction of particles is defined by the elastic Hertz contact force, i.e. Eq. (4) characterised with the effective stiffness K_{eff} according to Eq. (5) and by the viscoelastic damping force in Eq. (6) obtained according to Eq. (7) and characterised by the modified damping parameter $C_{\mathrm{mod},k}$ for each particular damping model k.

5.2. Numerical simulation of impact on mono-sized chain

5.2.1. Initial data

The free-end mono-sized granular chain consisting of $N_1 = 50$ equal spherical particles of radius $R_1 = 0.0127$ m (Fig. 8a) was considered. The striker presents identical spherical particle of radius $R_{str} = 0.0127$ m.

The mechanical properties of the stainless steel (grade 316) reported by Stevens and Hrenya [9] will be considered. They include the Young's modulus $E = 193$ GPa, Poisson's ratio $\nu = 0.35$ and density of material $\rho = 8030$ kg/m^3. The mass of particle is $m_p = 0.0689$ kg. The inter-particle contact properties are defined by the effective mass which is $m_{eff} = m_p/2 = 0.0345$ kg and the effective Hertz contact stiffness $K_{eff} = 1.17 \cdot 10^{10}$ kg s^{-2} m$^{-1/2}$. The damping properties of the contact are defined by the experimentally obtained values of COR (Fig. 7d), which were already discussed in the previous section.

When the striker collides at the first particle of a granular chain with the specified impact velocity $v_0 = 1.0$ m/s, the accumulated kinetic energy pushes particles, generates an inter-particle contact and initiates propagation of wave. Series of numerical experiments with different damping data were performed applying DEM during the time period up to 0.0022 s to illustrate the role of damping models in propagation of the force in granular chain after impact.

Evaluation of the coefficient of restitution and damping properties was discussed in previous section and was illustrated in Fig. 7. In the first sample, they were calculated by considering the simulation velocity equal to the impact velocity $v_{0,sim} = v_0 = 1.0$ m/s. Assuming this value as a reference velocity $v_{0,ref} = 1.0$ m/s, consequently $\lambda_{sim} = 1$, coefficient of restitution $e = 0.865$ was found from the experimental curve. Finally, the damping ratios $c_k(0.865)$ and the values of the modified damping constants $C_{\mathrm{mod},k}(e, v_{0,sim}) = C_{\mathrm{mod},k}(0.865, 1.0)$ are obtained as follows: $C_{\mathrm{mod},LH} = 1.10 \cdot 10$ kg s^{-1}, $C_{\mathrm{mod},LH} = 2.07 \cdot 10^3$ kg m$^{-1/4}$ s^{-1}, $C_{\mathrm{mod},KK} = 3.69 \cdot 10^4$ kg m$^{-1/2}$ s^{-1} and $C_{\mathrm{mod},HU} = 3.05 \cdot 10^9$ kg m$^{-3/2}$ s^{-1}.

Evaluation of velocity-dependent damping properties during multiple contacts in the propagation of wave is a complicated task. The samples are designed to illustrate contribution of damping during velocity decay. This phenomenon will be characterised by reducing the values of simulation velocity $v_{0,sim} = 0.7$ m/s and $v_{0,sim} = 0.5$ m/s will be examined. Two corresponding vales of COR, $e = 0.890$ and $e = 0.910$ are extracted from the experimental curve in Fig. 7d. Assuming $\lambda_{sim} = 1$ corresponding to $v_{0,sim} = 0.7$ m/s and $v_{0,ref} = 0.5$ m/s, evaluation of damping constants follows the same path as they were treated in the first sample.

Comparison of the vaults of the obtained damping constants indicates basic tendencies in the contribution of simulation velocity. The velocity independent TS model is characterised by sequentially increasing values $C_{\mathrm{mod},TS}(0.865) = 2.07 \cdot 10^3 < C_{\mathrm{mod},TS}(0.890) = 1.67 \cdot 10^3 < C_{\mathrm{mod},TS}(0.910) = 1.35 \cdot 10^3$ kg m$^{-1/4}$ s^{-1} that reflect an increase of the COR only. The damping of the other three models is contributed by the decaying values of simulation velocity is shown in Fig. 7. The velocity yields additional increase of damping for HU model $C_{\mathrm{mod},HU}(0.865) = 3.05 \cdot 10^9 < C_{\mathrm{mod},HU}(0.890) = 3.48 \cdot 10^9 C_{\mathrm{mod},HU}(0.910) = 3.91 \cdot 10^9$ and reduction for other KK and LH models, $C_{\mathrm{mod},KK}(0.865) = 3.69 \cdot 10^4 > C_{\mathrm{mod},KK}(0.890) = 3.13 \cdot 10^4 < C_{\mathrm{mod},KK}(0.910) = 2.69 \cdot 10^4$ and $C_{\mathrm{mod},LH}(0.865) = 1.1 \cdot 10^2 < C_{\mathrm{mod},LH}(0.890) = 8.29 \cdot 10 < C_{\mathrm{mod},LH}(0.910) = 6.27 \cdot 10$, respectively.

5.2.2. Results and discussion

Illustrations of the wave propagation are shown in Figs. 9 and 10. The model-dependent velocity wave is illustrated by velocity profiles obtained at the time instances $t = 0.001$ s and $t = 0.002$ s depicted in Fig. 9, where the profile curves are formed by the discrete values of velocities of $N = 50$ individual particles. Propagation of the force wave is demonstrated by variations of the inter-particle force between particles 49 and 50 in time depicted in Fig. 10.

Generally, velocity profiles (Fig. 9) illustrate the typical picture observed by considering the low-frequency waves relevant for the macroscopic dynamic behaviour of the granular solids [35]. Here, the dissipative contributions are proportional to the relative velocities of grains in elastic contact. The low-frequency waves have an amplitude-dependent propagation with wavelengths spanning in the case of a one-dimensional chain of uncompressed spheres of about 5–7 sphere diameters.

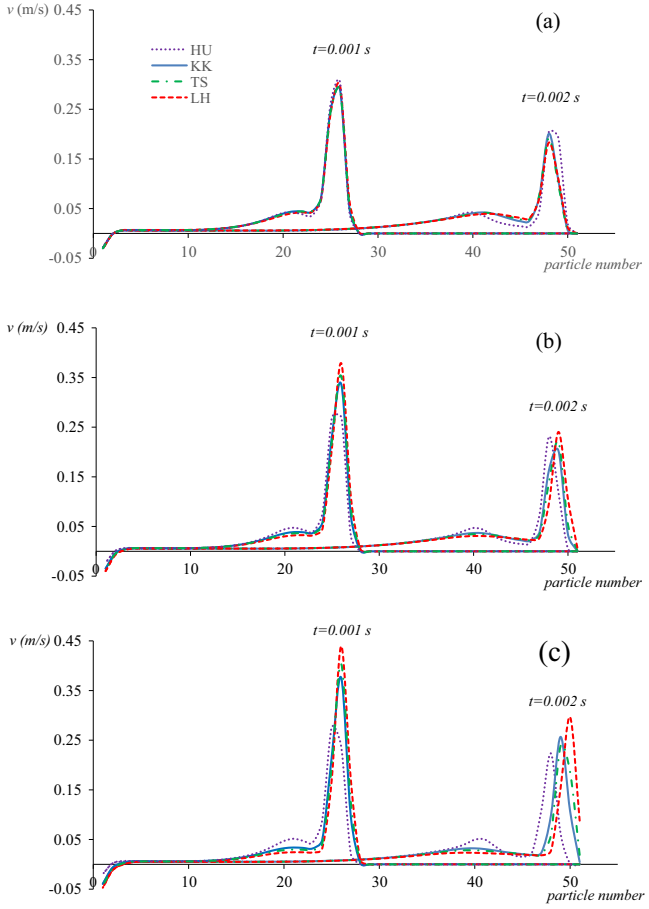

Fig. 9. Profiles of the velocity wave obtained for models at the fixed time instances $t = 0.001$ s and $t = 0.002$ s: (a) $e = 0.865$, $v_{0,sim} = v_{0,ref} = 1.0$ m/s; (b) $e = 0.890$, $v_{0,sim} = v_{0,ref} = 0.7$ m/s; (c) $e = 0.910$, $v_{0,sim} = v_{0,ref} = 0.5$ m/s.

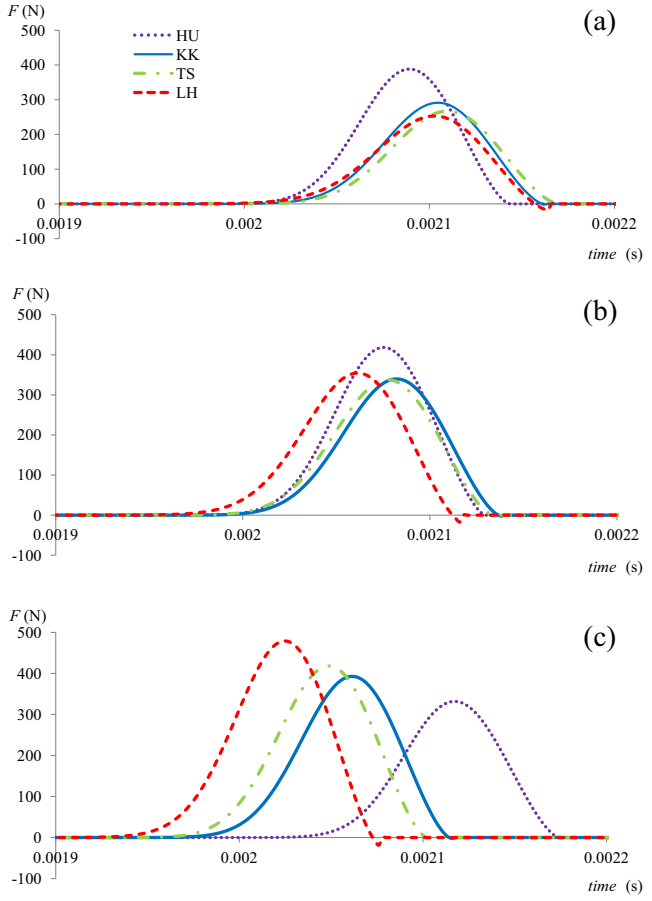

Fig. 10. Variations of the inter-particle force between particles 49 and 50: (a) $e = 0.865$, $v_{0,sim} = v_{0,ref} = 1.0$ m/s; (b) $e = 0.890$, $v_{0,sim} = v_{0,ref} = 0.7$ m/s; (c) $e = 0.910$, $v_{0,sim} = v_{0,ref} = 0.5$ m/s.

Each of the profiles is shown by four curves relevant to particular damping model. Two families of profile obtained in at the time instances $t = 0.001$ s and $t = 0.002$ s allow us to capture propagation character. In earlier stage difference between models is negligible. The differences in velocity amplitude increases while contacts number grows and initial contact velocity decreases and could by distinguished in the final stage (Fig. 9c).

The differences of the wave are coherent with the number of contacts, because every other contact has another initial velocity than which has been and that leads to $\lambda_{sim} \neq 1$. Taking into account energy lost during multiple contact, the final differences between models are very dependable of fitting point, when ($\lambda = 1.0$), while energy lost is directly reflected by COR. In Fig. 7d, it is possible to find that cases when $\lambda < 1.0$ and $\lambda > 1.0$ produce opposite energy dissipation difference while HU, KK and LH models are in use. This property is highly important if particles in particles system simulation can obtain velocities ($v_{0,sim}$) greater than one, which was used in the damping equation ($v_{0,ref}$). If this happens, then the final energy lost differences between models become smaller because opposite cases, while $\lambda < 1.0$ and $\lambda > 1.0$, compensate each other.

In Figs. 9 and 10 the aforementioned effect is clearly seen. Case a (Figs. 9 and 10) represents the decaying of λ_{sim} which leads to velocity, as well as contact force, distribution similar to distribution of COR in Fig. 7d when $v_0 < v_{0,ref}$. Cases b and c (Figs. 9 and 10) are obtained when $0 < \lambda \leqslant 1.0$, using Fig. 7d representation this would be similar to $0 < v_{0,ref} \leqslant v_0$. As we can see, case b is closest to set of parameters, which lead to lowest differences between models as well as to results of initial velocity independent Tsuji model.

5.3. Comparison with experiment

5.3.1. Initial data

The stepped chain is more complex compared to the mono-sized samples, therefore, the higher importance of such a comparison is expected. To evaluate the adequacy of various damping models to reality, the impact experiment of the stepped chain (Fig. 8b) reported by Job et al. [35] was considered. The initial data, material properties and available experiment data considered here were used below for the modelling purposes.

The first part of the stepped chain contains $N_1 = 7$ larger particles having radius $R_1 = 13.0$ mm, while the second part consists of $N_2 = 50$ smaller particles with radius $R_2 = 6.5$ mm. The radius of striker initially moving at velocity, $v_0 = 0.34$ m/s, is $R_{str} = 6.5$ mm.

Mechanical properties of the high carbon chrome hardened AISI 52100 steel roll bearings reported by Job et al. [35] will be considered. They include the Young's modulus $E = 203$ GPa, Poisson's ratio $\nu = 0.3$ and density of material $\rho = 7780$ kg/m^3. It could be noticed that the initial velocity and coefficient of restitution were not given in original paper; they were taken from [19], where the coefficient of restitution $e = 0.965$ was obtained after the fitting procedure.

The Hertz contact stiffness between two particles is obtained according to Eq. (5). Thereby, three stiffness values K_{eff} equal to: $8.67 \cdot 10^9$ kg m$^{-1/2}$ s^{-1}, $9.98 \cdot 10^9$ kg m$^{-1/2}$ s^{-1} and $1.23 \cdot 10^{10}$ kg m$^{-1/2}$ s^{-1} are obtained. These stiffness reflect contact between two equal 6.5 mm particles, two different 13.0 mm and 6.5 mm particles and two equal 13.0 mm particles, respectively. The masses of the particles are 0.0716 kg and 0.00895 kg for 13.0 mm and 6.5 mm particles, respectively.

The damping ratios $c_k(0.965)$ corresponding to this value of COR extracted from the graphs in Fig. 2, and the following values, $c_{LH}(0.965) = 0.018$, $c_{TS}(0.965) = 0.025$, $c_{KK}(0.965) = 0.026$ and $c_{HU}(0.965) = 0.062$ are obtained.

5.3.2. Results and discussion

Propagation of the force during the time period up to 3.0 ms was simulated by the DEM. Comparison of simulation results with the experiment in terms of the force time histories is given in Fig. 11. Two time histories of the contact force measured in experiment will be examined and shown hereafter. The variation of the inter-particle force transmitted by the seventh larger particle at the end of the larger chain is denoted as F_1. The force transmitted by the fiftieth particle evaluated at the end of the stepped chain is denoted F_2. Comparisons of simulation results with experiment in terms of the force time histories of the above force for each model are presented in Fig. 11.

In this problem, the initial impact is imposed by a light striker, therefore, a single wave (SW) propagates in the first part of chain Fig. 11. It is obvious that the simulation results are quite close to the experiment because the damping makes a minor influence while restitution coefficient was high. It can be seen that the experimentally obtained peak value $F_{1,\exp} = 110.0$ N is enveloped by the LH and KK models with $F_{1,KK} = 114.5$ N and $F_{1,LH} = 119.2$ N, respectively.

Later results clearly indicate that the heavier part of the stepped chain acts as impactor. Thus, a single wave observed at the end of a mono-sized chain of larger particles leads to the generation of a solitary wave train (SWT) in the second part of chain with smaller particles. The solitary wave trains phenomena has been discussed in earlier works [15,39].

It is obvious that the interrelation between models in the first peak practically replicates previous results and is similar to the results obtained for single particle impact. The values of the first peak are quite close to the experiment because the damping makes a minor influence while restitution coefficient was high. It is

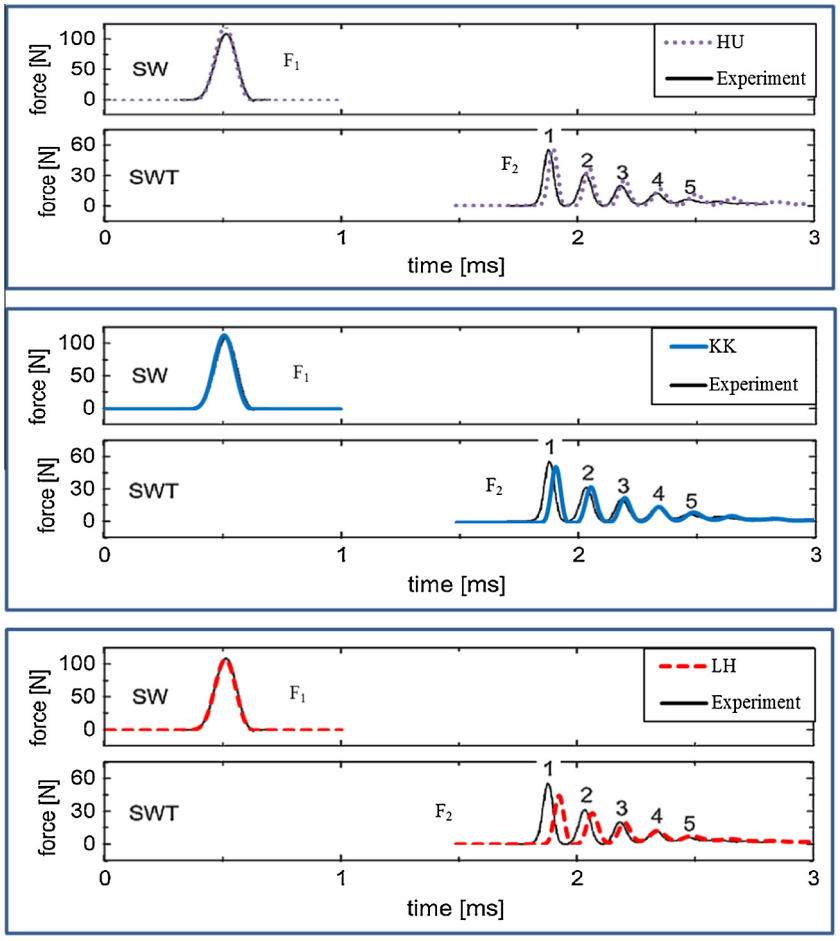

Fig. 11. Time histories illustrating the propagation of inter-particle forces in the stepped chain – comparison of simulation results ($e = 0.965$) for different models with the experiment [35].

obvious that experimentally obtained peak value $F_{1,exp} = 57.0$ N is enveloped by the HU and KK models with $F_{1,HU} = 57.0$ N and $F_{1,KK} = 51.6$ N values, respectively.

Our results illustrate that the simulation results yield to faster wave propagates with respect to experimentally observed reality. Moreover, further peaks decay slowly.

It was observed that the different damping models affect the propagation velocity of contact force in different ways. Explanations of this effect require however additionally investigation.

6. Conclusions

The theoretical analysis of four selected normal viscous damping models and numerical results obtained during single particle impact indicate that an increase of the displacement exponent at fixed values of the COR directly results into an increase of inter-particle forces. Thereby, actual scattering of maximum force values is restricted with the lower bound yielded by the LH model and with the upper bound yielded by the HU model. At high damping characterised by the values of COR close to unity $e > 0.9$ the difference between models may be negligible.

The general form of viscoelastic damping models shows the influence of the impact velocity used for evaluation of damping parameter. Different signs of velocity exponent $\beta_{v,k}$ ($\beta_{v,k} > = < 0$) indicate different sensitivities of particular damping models with respect to impact velocity. More precisely, this contribution is expressed in terms of the differences between the simulation impact velocities used for the calculation of damping constants and the actual impact velocities of individual particles. In practical situations, this effect may result in different speeds of wave and into reverse of force bounds between LH and HU models.

Acknowledgements

Partial financial support by the DFG, Germany, through Grant KR3446/6-1 is acknowledged.

This research was funded by a Grant (No. Nr. MIP-072/2013) from the Research Council of Lithuania and by Vilnius Gediminas Technical University, Lithuania.

References

[1] P. Cundall, O. Strack, A discrete numerical model for granular assemblies, Geotechnique 29 (1979) 47–65.
[2] K.L. Johnson, Contact Mechanics, first ed., Cambridge University Press, Cambridge, 1987.
[3] P. Wriggers, Computational Contact Mechanics, second ed., Springer, Berlin, 2006.
[4] H.-G. Matuttis, J. Chen, Understanding the Discrete Element Method: Simulation of Non-Spherical Particles for Granular and Multi-body Systems, Wiley, Singapore, 2014.
[5] J. Schäfer, S. Dippel, D.E. Wolf, Force schemes in simulations of granular materials, J. Phys. I Fr. 6 (1996) 5–20.
[6] A. Džiugys, B. Peters, An approach to simulate the motion of spherical and non-spherical fuel particles in combustion chambers, Granul. Matter 3 (2001) 231–266.
[7] Y. Zhang, B. Jin, W. Zhong, B. Ren, R. Xiao, DEM simulation of particle mixing in flat-bottom spout-fluid bed, Chem. Eng. Res. Des. 88 (2010) 757–771.

[8] G. Lu, J.R. Third, C.R. Müller, Discrete element models for non-spherical particle systems: from theoretical developments to applications, Chem. Eng. Sci. 127 (2015) 425–465.
[9] A.B. Stevens, C.M. Hrenya, Comparison of soft-sphere models to measurements of collision properties during normal impacts, Powder Technol. 154 (2005) 99–109.
[10] H. Kruggel-Emden, E. Simsek, S. Rickelt, S. Wirtz, V. Scherer, Review and extension of normal force models for the discrete element method, Powder Technol. 171 (2007) 157–173.
[11] C.-Y. Wu, L.-Y. Li, C. Thornton, Energy dissipation during normal impact of elastic and elastic–plastic spheres, Int. J. Impact Eng 32 (2005) 593–604.
[12] T. Schwager, T. Pöschel, Coefficient of restitution and linear–dashpot model revisited, Granul. Matter 9 (2007) 465–469.
[13] D. Zhang, W.J. Whiten, The calculation of contact forces between particles using spring and damping models, Powder Technol. 88 (1996) 59–64.
[14] J. Lee, H. Herrmann, Angle of repose and angle of marginal stability: molecular dynamics of granular particles, J. Phys. A: Math. Gen. 26 (1999) 373–383.
[15] G. Kuwabara, K. Kono, Restitution coefficient in a collision between two spheres, Jpn. J. Appl. Phys. 26 (1987) 1230–1233.
[16] N.V. Brilliantov, F. Spahn, J.-M. Hertzsch, T. Pöschel, Model for collisions in granular gases, Phys. Rev. E 53 (1996) 5382–5392.
[17] Y. Tsuji, T. Tanaka, T. Ishida, Lagrangian numerical simulation of plug flow of cohesionless particles in a horizontal pipe, Powder Technol. 71 (1992) 239–250.
[18] G. Hu, Z. Hu, B. Jian, L. Liu, H. Wan, On the determination of the damping coefficient of non-linear spring-dashpot system to model hertz contact for simulation by discrete element method, J. Comput. 6 (2011) 984–988.
[19] H.-G. Matuttis, Simulation of the pressure distribution under a two-dimensional heap of polygonal particles, Granul. Matter 1 (1998) 83–91.
[20] K.H. Hunt, F.R.E. Crossley, Coefficient of restitution interpreted as damping in vibroimpact, J. Appl. Mech. 7 (1975) 440–445.
[21] R. Ramirez, T. Pöschel, N. Brilliantov, T. Schwager, Coefficient of restitution of colliding viscoelastic spheres, Phys. Rev. E 60 (1999) 4465–4472.
[22] S. Luding, E. Clément, A. Blumen, J. Rajchenbach, J. Duran, Anomalous energy dissipation in molecular-dynamics simulations of grains: the "detachment" effect, Phys. Rev. E 50 (1994) 4113–4122.
[23] A. Rosas, J. Buceta, K. Lindenberg, Dynamics of two granules, Phys. Rev. E 68 (2003) 021303.
[24] D. Antypov, J. Elliott, On an analytical solution for the damped Hertzian spring, EPL Europhys. Lett. 94 (2011) 50004.
[25] K.F. Malone, B.H. Xu, Determination of contact parameters for discrete element method simulations of granular systems, Particuology 6 (2008) 521–528.
[26] M. Gharib, Y. Hurmuzlu, A new contact force model for low coefficient of restitution impact, J. Appl. Mech. 79 (2012) 064506.
[27] S. Ray, T. Kempe, J. Fröhlich, Efficient modelling of particle collisions using a non-linear viscoelastic contact force, Int. J. Multiph. Flow 76 (2015) 101–110.
[28] C.X.X. Wong, M.C.C. Daniel, J.A. Rongong, Energy dissipation prediction of particle dampers, J. Sound Vib. 319 (2009) 91–118.
[29] Z. Lu, S.F. Masri, X. Lu, Parametric studies of the performance of particle dampers under harmonic excitation, Struct. Control Health Monit. 18 (2011) 79–98.
[30] C.M.M. Wensrich, R.E.E. Stratton, Shock waves in granular materials: discrete and continuum comparisons, Powder Technol. 210 (2011) 288–292.
[31] C.N. Thomasa, S. Papargyri-Beskoub, G. Mylonakis, Wave dispersion in dry granular materials by the distinct element method, Soil Dyn. Earthq. Eng. 29 (2009) 888–897.
[32] N. Zamani, U. El Shamy, Analysis of wave propagation in dry granular soils using DEM simulations, Acta Geotech. 6 (2011) 167–182.
[33] Y. Wang, C.M. Wensrich, J.Y. Ooi, Rarefaction wave propagation in tapered granular columns, Chem. Eng. Sci. 71 (2012) 32–38.
[34] H. Kruggel-Emden, F. Stepanek, A. Munjiza, A study on adjusted contact force laws for accelerated large scale discrete element simulations, Particuology 8 (2010) 161–175.
[35] S. Job, F. Melo, A. Sokolow, S. Sen, Solitary wave trains in granular chains: experiments, theory and simulations, Granul. Matter 10 (2007) 13–20.
[36] V. Nesterenko, C. Daraio, E. Herbold, S. Jin, Anomalous wave reflection at the interface of two strongly nonlinear granular media, Phys. Rev. Lett. 95 (2005) 158702.
[37] F. Melo, S. Job, F. Santibanez, F. Tapia, Experimental evidence of shock mitigation in a Hertzian tapered chain, Phys. Rev. E 73 (2006) 041305.
[38] F. Santibanez, R. Munoz, A. Caussarieu, S. Job, F. Melo, Experimental evidence of solitary wave interaction in Hertzian chains, Phys. Rev. E 84 (2011) 026604.
[39] S. Luding, E. Clément, A. Blumen, Studies of columns of beads under external vibrations, Phys. Rev. E 49 (1994) 1634–1646.
[40] N. Nguyen, B. Brogliato, Shock dynamics in granular chains: numerical simulations and comparison with experimental tests, Granul. Matter 14 (2012) 341–362.
[41] U. Harbola, A. Rosas, M. Esposito, K. Lindenberg, Pulse propagation in tapered granular chains: an analytic study, Phys. Rev. E 80 (2009) 031303.
[42] C. Daraio, V. Nesterenko, E. Herbold, S. Jin, Strongly nonlinear waves in a chain of Teflon beads, Phys. Rev. E 72 (2005) 016603.
[43] B.P. Lawney, S. Luding, Frequency filtering in disordered granular chains, Acta Mech. 225 (2014) 2385–2407.
[44] R. Kačianauskas, H. Kruggel-Emden, E. Zdancevičius, D. Markauskas, Critical assessment of visco-elastic damping models used in DEM simulations, Procedia Eng. 7th World Congr. Part. Technol. 102 (2015) 1415–1425.
[45] R. Balevičius, A. Džiugys, R. Kačianauskas, A. Maknickas, K. Vislavičius, Investigation of performance of programming approaches and languages used for numerical simulation of granular material by the discrete element method, Comput. Phys. Commun. 175 (2006) 404–415.
[46] R. Balevičius, R. Kačianauskas, Z. Mróz, I. Sielamowicz, Microscopic and macroscopic analysis of granular material behaviour in 3d flat-bottomed hopper by the discrete element method, Arch. Mech. 59 (2007) 231–257.
[47] D. Zabulionis, R. Kačianauskas, D. Markauskas, J. Rojek, An investigation of nonlinear tangential contact behaviour of a spherical particle under varying loading, Bull. Polish Acad. Sci. Tech. Sci. 60 (2012) 265–278.
[48] H. Kruggel-Emden, M. Sturm, S. Wirtz, V. Scherer, Selection of an appropriate time integration scheme for the discrete element method (DEM), Comput. Chem. Eng. 32 (2008) 2263–2279.
[49] T. Pöschel, C. Salueña, T. Schwager, Scaling properties of granular materials, Phys. Rev. E 64 (2001) 011308.
[50] M. Van Zeebroeck, E. Tijskens, P. Van Liedekerke, V. Deli, J. de Beaerdemaeker, H. Ramon, et al., Determination of the dynamical behaviour of biological materials during impact using a pendulum device, J. Sound Vib. 266 (2003) 465–480.
[51] S. McNamara, E. Falcon, Simulations of vibrated granular medium with impact-velocity-dependent restitution coefficient, Phys. Rev. E 71 (2005) 031302.